PREPRINT
Preprint typeset using LaTeX style emulateapj v. 6/22/04

MID-INFRARED SPECTROSCOPY OF CARBON STARS IN THE SMALL MAGELLANIC CLOUD

G. C. SLOAN[1], K. E. KRAEMER[2], M. MATSUURA[3,4], P. R. WOOD[5], S. D. PRICE[2], M. P. EGAN[6]

PREPRINT

ABSTRACT

We have observed a sample of 36 objects in the Small Magellanic Cloud (SMC) with the Infrared Spectrometer on the *Spitzer Space Telescope*. Nineteen of these sources are carbon stars. An examination of the near- and mid-infrared photometry shows that the carbon-rich and oxygen-rich dust sources follow two easily separated sequences. A comparison of the spectra of the 19 carbon stars in the SMC to spectra from the *Infrared Space Observatory* (*ISO*) of carbon stars in the Galaxy reveals significant differences. The absorption bands at 7.5 μm and 13.7 μm due to C_2H_2 are stronger in the SMC sample, and the SiC dust emission feature at 11.3 μm is weaker. Our measurements of the MgS dust emission feature at 26–30 μm are less conclusive, but this feature appears to be weaker in the SMC sample as well. All of these results are consistent with the lower metallicity in the SMC. The lower abundance of SiC grains in the SMC may result in less efficient carbon-rich dust production, which could explain the excess C_2H_2 gas seen in the spectra. The sources in the SMC with the strongest SiC dust emission tend to have redder infrared colors than the other sources in the sample, which implies more amorphous carbon, and they also tend to show stronger MgS dust emission. The weakest SiC emission features tend to be shifted to the blue; these spectra may arise from low-density shells with large SiC grains.

Subject headings: circumstellar matter — infrared: stars — stars: carbon — Magellanic Clouds

1. INTRODUCTION

The formation of CO in the cool atmospheres of stars on the asymptotic giant branch (AGB) forces the chemistry of the dust produced by mass-losing stars to be either oxygen-rich or carbon-rich, depending on whether the C/O ratio in these stars is less than or more than one. In the Galaxy, AGB stars are the primary source of material injected into the interstellar medium (ISM) (Gehrz 1989), and they are predominantly oxygen-rich (see the statistics of the characterizations of spectra from the *IRAS* Low-Resolution Spectrometer by the *IRAS* Science Team 1986). Consequently, carbon-rich dust species are a small fraction of the material injected into the galactic ISM compared to silicates and related oxygen-rich dust species.

The Large Magellanic Cloud (LMC) has a higher fraction of carbon stars than the Galaxy (Blanco et al. 1978), and the Small Magellanic Cloud (SMC) has a higher fraction still (Blanco et al. 1980). Renzini & Voli (1981) showed that reducing the initial metallicity of a star increases the likelihood that it will become a carbon star on the AGB. More metal-poor stars have less oxygen in their atmospheres initially, so once they begin to dredge up carbon-rich material from the interior, fewer dredge-ups are needed to raise the C/O ratio past unity (Lattanzio & Wood 2004). As a result, the mass limit above which stars will evolve into carbon stars decreases as metallicity decreases. In the models with Z=0.02 examined by Renzini & Voli (1981), the limit is $\sim$1.8 $M_{\odot}$ (depending on other assumptions), but for Z=0.004, the limit is $\sim$1.3 $M_{\odot}$.

Thus, in low-metallicity galaxies, more of the dust injected into the ISM from AGB stars will be carbon-rich. The *Spitzer Space Telescope* (Werner et al. 2004) can observe fainter, more distant, and more metal-poor galaxies than previous infrared telescopes, which makes it essential to better understand the nature of the dust produced in these systems. The sensitivity of the Infrared Spectrograph (IRS, Houck et al. 2004) on *Spitzer* makes it possible to obtain spectra of a large sample of individual dust shells around evolved stars in the Magellanic Clouds. The metallicity of the younger population in the SMC is $\sim$0.2 Solar (Russell & Bessell 1989; Hill et al. 1997; Luck et al. 1998). The sources which populate the AGB are older and may even be more metal poor. Thus the SMC is an ideal laboratory for studying how metallicity affects the nature of carbon-rich dust produced on the AGB.

We have used the IRS to observe a sample of 36 infrared sources in the SMC, most of which are evolved stars. Nineteen of these sources are carbon-rich AGB sources. In this paper, we will compare their spectroscopic properties to the Galactic sample of carbon stars, as observed by the Short-Wavelength Spectrometer (SWS) aboard *ISO*. The spectra from carbon stars in the wavelength range covered by both instruments include both emission features from dust and absorption features from molecular gas.

Gilman (1969) predicted that the dominant condensates in the outflows of carbon stars would be carbon (later specified as graphite or amorphous carbon) and silicon carbide. Hackwell (1972) first observed an emission feature at 11.3 μm in the carbon stars V Hya and CIT 6. Treffers & Cohen (1974) confirmed the presence of this feature in spectra of CIT 6 and IRC +10216, and they identified its carrier as SiC dust. Amorphous carbon dominates the dust produced by heavily reddened carbon stars, as shown by models of the spectral energy distribution of the extreme carbon star IRC +10216 (e.g.,

[1] Cornell University, Astronomy Department, Ithaca, NY 14853-6801, sloan@isc.astro.cornell.edu
[2] Air Force Research Laboratory, Space Vehicles Directorate, 29 Randolph Road, Hanscom AFB, MA 01731, kathleen.kraemer@hanscom.af.mil, steve.price@hanscom.af.mil
[3] School of Physics and Astronomy, University of Manchester, P.O. Box 88, Sackville Street, Manchester M60 1QD, United Kingdom
[4] Department of Physics and Astronomy, Queen's University of Belfast, Belfast BT7 1NN, Northern Ireland, United Kingdom, m.matsuura@qub.ac.uk
[5] Research School of Astronomy and Astrophysics, Australian National University, Cotter Road, Weston Creek ACT 2611, Australia, wood@mso.anu.edu.au
[6] Air Force Research Laboratory, Space Vehicles Directorate, 1851 S. Bell St., CM3, Suite 700, Arlington, VA 22202, michaelegan.cox.net

Martin & Rogers 1987; Griffin 1990; Sloan & Egan 1995).

Goebel & Moseley (1985) identified MgS dust as the carrier of a broad emission feature first observed spectroscopically in the 26–30 μm range by Forrest et al. (1981) in the shells around heavily reddened carbon stars. SWS observations of Galactic carbon stars served as the basis for a thorough study by Hony et al. (2002). They found a wide variation in the shape of the feature, which they explained on the basis of grain temperature. Their ability to fit a variety of spectral feature shapes using MgS considerably strengthens its identification as the carrier of the 26–30 μm feature.

In addition to the dust features, the IRS wavelength range also includes two molecular bands seen in carbon-rich spectra. The narrow band at 13.7 μm is well characterized and arises from acetylene (C_2H_2), specifically from the Q branch of the ν_5 band (Aoki et al. 1999). The P and R branches produce broad shoulders to this narrow feature which typically absorb in the 12.5–15.0 μm range. The identification of the band at 7.5 μm is more problematic, as HCN, C_2H_2, and CS all absorb in this spectral region (Aoki et al. 1998; Jørgensen et al. 2000). Matsuura et al. (2006) argue that C_2H_2 is the dominant absorber, based on the similarity of its expected band shape and position to the observed band in carbon stars in the LMC. Matsuura et al. (2006) also show that the HCN band at 14.1 μm seen in Galactic carbon stars is absent in the LMC sample. It does not appear in our SMC sample, either.

2. OBSERVATIONS

2.1. *The spectral data*

The *Spitzer Space Telescope* observed all of the sources in our sample at low resolution (R$\sim$60–120), using the standard IRS staring mode. The integration times for both the Short-Low (SL) and Long-Low (LL) modules are split evenly between the first- and second-order apertures. Table 1 presents the observational details along with photometry at J and K_s from 2MASS and *MSX* band A (8.3 μm).

The analysis began with the two-dimensional flatfielded images produced by version S11.0 of the data reduction pipeline at the *Spitzer* Science Center (SSC)[7]. We subtracted sky images to remove any background emission. SL images were differenced aperture-by-aperture (i.e. SL1$-$SL2 and vice versa), and LL images were differenced nod-by-nod. Before extracting spectra from the images, we used the *imclean* software package distributed by Cornell University[8] to replace bad pixels with values determined from neighboring pixels.

To extract spectra from the cleaned and differenced images, we used the SSC pipeline modules *profile*, *ridge* and *extract*, which are available through SPICE (the Spitzer IRS Custom Extractor, distributed by the SSC). To photometrically calibrate the spectra, we used spectral corrections generated from observations of standard stars. For SL, we used HR 6348 (K0 III), and for LL, we used HR 6348, HD 166780 (K4 III) and HD 173511 (K5 III). The assumed truth spectra of these spectra are modified from spectral templates provided by M. Cohen. A paper explaining this process is in preparation (Sloan et al.). We have used the modified wavelength calibration of the S11.0 version of the SSC pipeline described by Sloan et al. (2005).

After calibrating the spectra, we co-added them, stitched

[7] One source, MSX SMC 093, was observed later and processed with the S12.0 version of the pipeline.

[8] An updated version of this package, now known as *irsclean*, is available from the SSC website.

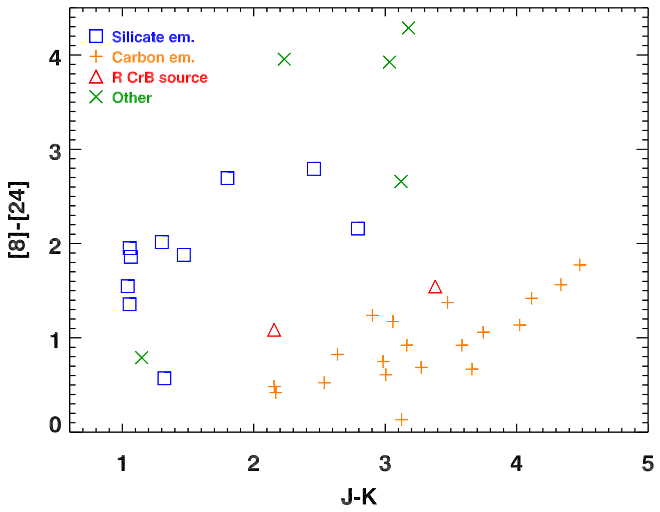

FIG. 1.— A color-color plot of the SMC sample. Plotting mid-infared colors vs. near-infrared colors separates the various dust compositions cleanly. This example uses 2MASS colors on the horizontal axis and colors derived from our IRS spectra using the bandpasses for the IRAC 8 μm and MIPS 24 μm filters on the *Spitzer Space Telescope*. The carbon-rich dust sources fall along a clear sequence which is red in J$-$K but blue in [8]$-$[24] compared to the oxgyen-rich sources.

the individual spectral segments together to correct discontinuities by making scalar multiplicative corrections, and trimmed poor data from the ends of the segments. The discontinuities arise primarily from variations in throughput caused by pointing variations, since a source will be better centered in some apertures than in others. Typical multiplicative corrections varied between 5 and 10%. Segments are normalized upwards to align with the best-centered segment. We have used the bonus-order data in SL and LL by combining it with orders 1 and 2 where they overlap and are valid. The error bars are the statistical differences between the two nod positions.

2.2. *The full sample*

Our full *Spitzer*/IRS sample consists of 36 infrared sources in the SMC. They were selected on the basis of near-infrared colors observed in the 2MASS survey (Skrutskie et al. 2006) and mid-infrared measurements from the *Midcourse Space Experiment* (*MSX*, Egan et al. 2003). The use of the 2MASS survey introduces a selection effect against heavily enshrouded sources, since reddening from the dust shell could push the near-infrared colors below the 2MASS detection limit of K$\sim$16. The MSX sensitivity limits the sample to magnitudes at 8 μm brighter than $\sim$8.5, which selects against sources with little dust.

The first objective of the program was to validate the spectroscopic properties predicted from the near-infrared and *MSX* colors for a sample of sources in the LMC (Egan et al. 2001). Out of the 36 targets in the SMC, 22 show infrared spectral features from carbon-rich dust or gas species. This fraction is higher than expected, primarily because the reddest J$-$K sources selected had been tentatively identified as OH/IR stars. They turned out to be embedded carbon stars instead. As a result, our sample of carbon stars covers a wide range of infrared colors.

Figure 1 illustrates how a combination of 2MASS and *Spitzer* photometry can distinguish the dust composition in

TABLE 1
SOURCES AND OBSERVING INFORMATION

MSX SMC	RA J2000.0	Dec. J2000.0	2MASS[a] J	2MASS[a] K_s	MSX A[b]	Integration time (s) SL	Integration time (s) LL
033	00 47 05.52	−73 21 33.0	13.445	10.320	7.320	112	168
036	00 45 53.95	−73 23 41.2	15.074	11.599	7.999	240	960
044	00 43 39.58	−73 14 57.6	12.567	10.031	7.752	112	240
054	00 43 05.90	−73 21 40.6	16.597	12.573	7.794	240	480
060	00 46 40.43	−73 16 47.2	15.680	11.199	6.150	112	112
062	00 42 40.91	−72 57 05.8	13.220	10.163	6.821	112	112
066	00 48 52.51	−73 08 56.8	14.699	11.115	7.184	240	360
091	00 36 56.71	−72 25 17.6	13.684	10.782	7.948	112	240
093	00 59 23.36	−73 56 01.0	14.419	11.414	7.840	240	960
105	00 45 02.15	−72 52 24.3	15.305	11.192	6.813	112	240
142	00 51 40.47	−72 57 29.0	12.902	10.734	8.032	112	360
159	00 54 22.29	−72 43 29.7	16.050	11.713	7.357	240	360
162	00 52 40.18	−72 47 27.7	12.482	9.846	7.375	112	168
163	00 51 00.75	−72 25 18.6	14.735	10.989	7.304	240	480
198	00 57 10.98	−72 31 00.0	14.692	11.418	7.719	240	960
200	00 46 50.79	−71 47 39.3	15.120	11.460	7.800	240	960
202	00 53 10.14	−72 11 54.7	11.930	9.775	7.967	112	240
209	00 56 16.39	−72 16 41.3	13.771	10.606	7.222	112	168
232	01 06 03.30	−72 22 32.3	14.302	11.318	7.317	240	480

[a]From Skrutskie et al. (2006).
[b]Magnitude at 8.3 μm; from Egan et al. (2003)

evolved stars. The [8]−[24] color is based on synthetic photometry of the IRS spectra using the bandpasses for the IRAC 8 μm and the MIPS 24 μm filters. The carbon-rich dust sources occupy a clear seqence with the [8]−[24] color steadily increasing from ∼0 to ∼2 as the J−K color increases from ∼2 to ∼5. The oxygen-rich sources occupy a different sequence with J−K colors ∼1.0–1.5 for [8]−[24] $\lesssim$2 and showing a wide range in J−K for redder [8]−[24] colors. At no point in Figure 1 do the two sequences overlap. Van Loon et al. (1997) showed that plotting K−[12] vs. J−K produces two separate sequences for the carbon-rich and oxygen-rich dust sources. Shifting the longer-wavelength color further to the infrared, as Figure 1 does here, eliminates the overlap between the sequences.

Two of the 22 carbon-rich sources exhibit featureless spectra resembling ∼600–700 K blackbodies. As described by Kraemer et al. (2005), they are R CrB candidates and are thus not associated with the AGB. These sources appear as triangles in Figure 1, and they lie slightly above the carbon-rich sequence. One of the carbon-rich sources shows PAH emission features superimposed on an otherwise smooth continuum peaking in the mid-infared. Kraemer et al. (in preparation) examine this source in a separate paper and conclude it has most likely evolved off of the AGB. It is plotted as one of the "Other" sources in Figure 1. The remaining 19 sources constitute our sample of carbon-stars in the SMC.

2.3. *The carbon stars*

Figure 2 presents the IRS low-resolution spectra of the 19 carbon stars in our sample from the SMC. All of these sources exhibit spectral characteristics typical of carbon stars on the AGB, including molecular absorption bands from C_2H_2 at 7.5 and 13.7 μm and the SiC dust emission feature at 11.3 μm. A few of the spectra also show a MgS dust emission feature peaking in the 26–30 μm range. Eighteen of the sources were observed in 2004 November; one object, MSX SMC 093, was observed in 2005 June. Figure 2 organizes the spectra by their [6.4]−[9.3] color, as defined in §3.1.

2.4. *Ground-based observations*

All of the carbon stars in our sample were observed from the ground quasi-simultaneously with the *Spitzer* observations. Near-infrared photometric observations were taken with the 2.3-m Telescope at Siding Spring Observatory (SSO) in Australia, using the near-infrared imaging system CASPIR (McGregor et al. 1994) and the filters J (effective wavelength 1.24 μm), H (1.68 μm), K (2.22 μm), and narrowband L (3.59 μm). Standard stars from the lists by McGregor (1994) were used to calibrate the observations. Standard image reduction procedures of bias subtraction, linearization, bad pixel replacement, flat fielding and sky subtraction were done using *IRAF*. Aperture photometry was performed with the *IRAF* task *QPHOT*. All objects were observed twice and the photometry averaged.

Table 2 presents the ground-based photometry for our sample. The errors given are the worst of the noise estimate from *QPHOT* or the standard error computed from the two observations. The 18 sources observed in 2004 November by *Spitzer* were observed four weeks later at SSO. MSX SMC 093 was observed by *Spitzer* on 2005 June 4. The photometric data in Table 2 for this source are linearly interpolated from SSO data obtained on May 25 and July 22.

Of the 19 carbon stars in our sample, 14 have light curves in the databases produced by the MACHO Project (Massive Compact Halo Objects; Alcock et al. 1996) and/or the Optical Gravitational Lensing Experiment (OGLE; Udalski et al. 1997; Szymánski 2005). Figure 3 presents these lightcurves. These stars all show evidence of pulsation, with a typical period of ∼300–700 days, making them large-amplitude, long-period variables.

These variables are typical of large-amplitude, dust enshrouded stars found in the Magellanic Clouds and the Galaxy (Whitelock et al. 2003; Lattanzio & Wood 2004). As well as the main pulsation period of ∼300–700 days, they often show long periods of dimming and brightening of many thousands of days (MSX SMC 060, 062, 142, 162, 232) and double-humped light curves, i.e. alternate faint and bright minima

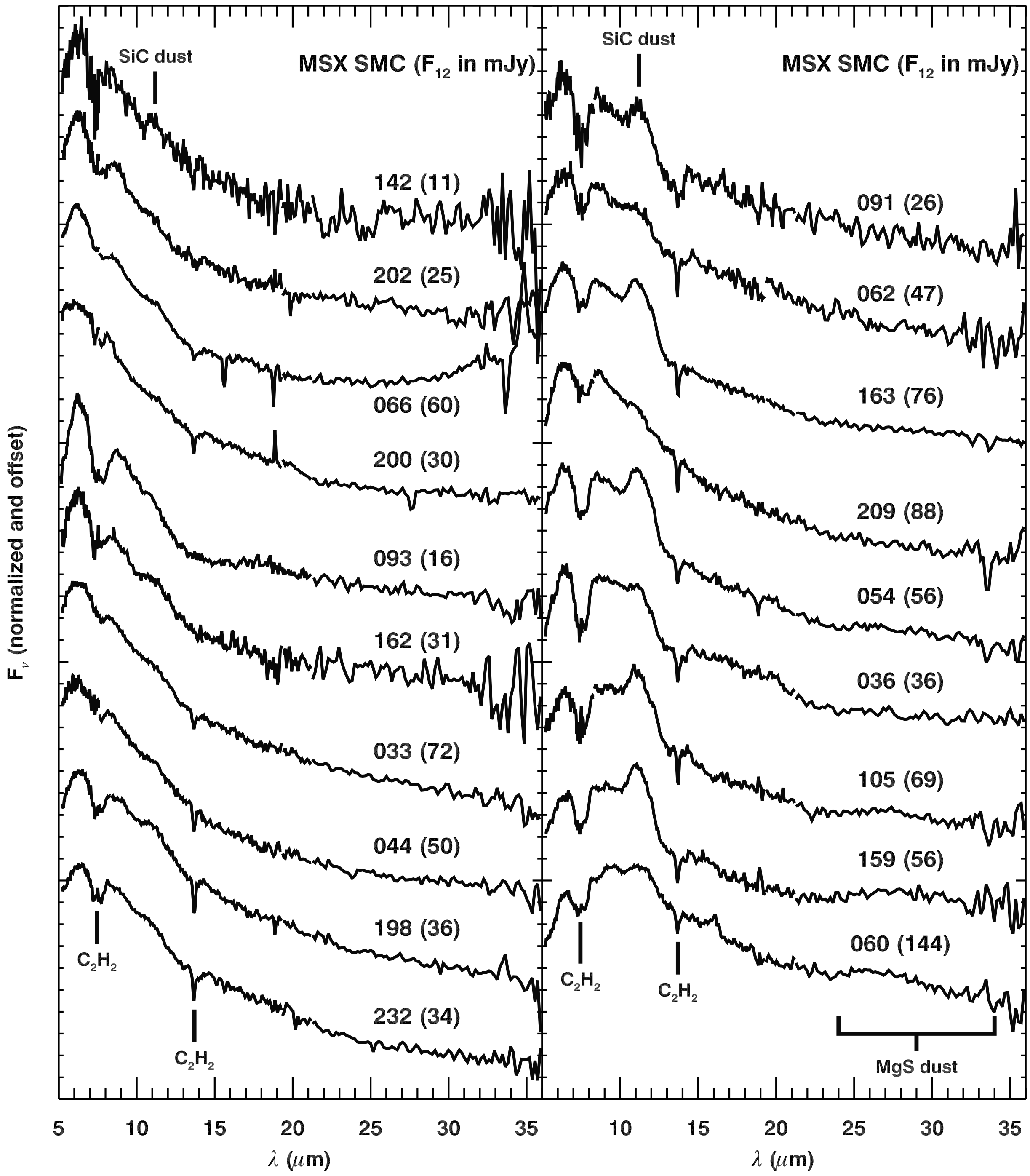

FIG. 2.— Our sample of mid-infrared spectra from carbon stars in the SMC. The dominant features are the C_2H_2 absorption bands at 7.5 and 13.7 μm, the SiC dust emission feature at 11.3 μm, and the MgS dust emission feature in the 26–30 μm range. The spectra are ordered by [6.4]−[9.3] color and normalized. The 12 μm flux in mJy is included in parentheses after the *MSX* SMC number of each source. Some of the spectra show artifacts due to background emission from forbidden lines that did not fully cancel out in the differenced images (most notably MSX SMC 066, with artifacts from [Ne III] at 15.6 μm and [S III] at 18.7 and 33.5 μm). Other artifacts appear due to unflagged misbehaving (i.e. rogue) pixels.

(MSX SMC 033, 066, 209). Olivier & Wood (2005) find this latter effect in their models of large-amplitude pulsating giants.

Our carbon stars are very red and fainter in K than stars of similar bolometric luminosity, but with shorter period and lower mass-loss rate, and as a result, on the K-log$P$ diagram, they typically lie on a very steep sequence of declining K magnitude at the long-period end of the sequence for fundamental mode pulsators (Miras) (Wood 1998, 2003; Lattanzio & Wood 2004). Once the heavy mass-loss phase begins, the period increases greatly due to the reduced mass while M_{bol} changes very little (Vassiliadis & Wood 1993). Thus the brightening in M_{bol} with log$P$ seen for stars with low mass-loss rates no longer holds and the sources in Table 2 no longer

TABLE 2
PHOTOMETRIC RESULTS

MSX SMC	J (mag)	H (mag)	K (mag)	L (mag)	period (days)	L_{bol} ($L_\odot$)
033	14.362±0.022	12.404±0.014	10.846±0.008	8.775±0.042	530	20090
036	···	14.400±0.024	12.711±0.028	10.373±0.095	640	5480
044	15.579±0.156	13.595±0.025	11.806±0.009	9.533±0.087	460	11780
054	16.516±0.325	14.326±0.044	12.247±0.012	9.841±0.223	···	8000
060	15.011±0.035	12.864±0.016	11.048±0.007	9.119±0.052	350	17520
062	15.343±0.033	13.235±0.019	11.581±0.009	9.501±0.060	570	9120
066	13.305±0.027	11.591±0.013	10.263±0.007	8.574±0.058	530	6300
091	15.311±0.077	13.334±0.031	11.654±0.011	9.917±0.145	···	5110
093	13.053±0.022	11.516±0.034	10.403±0.032	9.133±0.080	···	8210
105	16.082±0.129	13.687±0.024	11.783±0.009	9.540±0.046	670	9120
142	14.129±0.021	12.615±0.036	11.404±0.008	10.479±0.227	300	5180
159	17.398±0.199	15.010±0.078	12.656±0.017	9.534±0.070	560	7470
162	13.850±0.019	11.963±0.025	10.575±0.007	8.986±0.113	520	11480
163	15.528±0.044	13.280±0.040	11.526±0.023	9.266±0.090	660	13000
198	14.659±0.035	12.865±0.016	11.442±0.015	9.355±0.099	500	7810
200	16.697±0.086	14.182±0.020	12.207±0.025	9.736±0.074	···	9130
202	12.974±0.017	11.415±0.013	10.423±0.011	8.998±0.044	···	11460
209	14.035±0.025	12.147±0.014	10.795±0.007	8.908±0.042	520	16330
232	15.539±0.085	13.726±0.042	12.029±0.024	9.726±0.286	460	7280

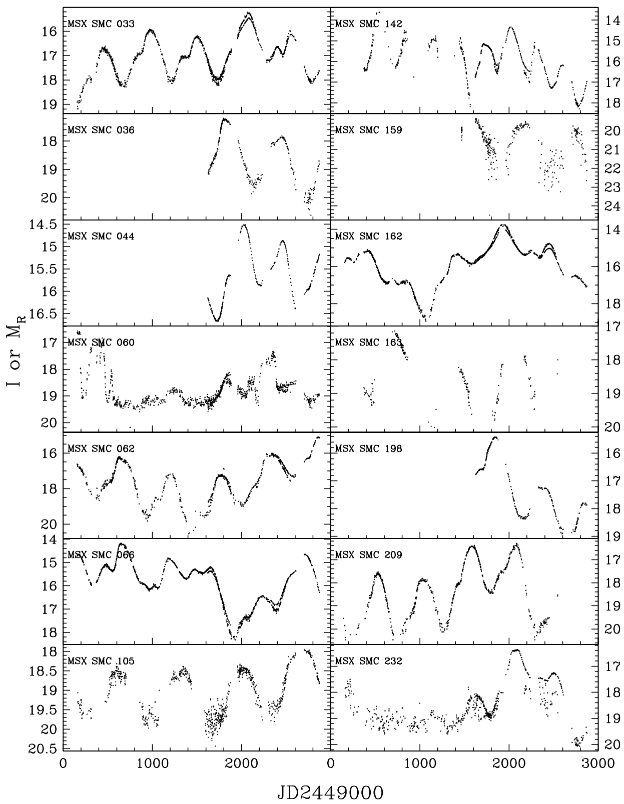

FIG. 3.— Light curves for the *Spitzer* sources which could be found in the MACHO and/or OGLE databases. JD2449000 is Julian Date−2449000 (days). The MACHO data extend over the time interval 100 < JD2449000 < 2600, while the OGLE data cover the time interval 1600 < JD2449000 < 2900. When both MACHO and OGLE data exist for a star, the zero point of the MACHO R magnitudes M_R has been adjusted so that the OGLE I magnitudes and MACHO R magnitudes match on average.

fall along a well-defined sequence, even in a plot of M_{bol} vs. $\log P$.

It should be remembered that there is a selection effect operating here which almost certainly acts to limit the maximum period seen in the optical databases. As the stars lose mass, their pulsation periods will increase and grow more violent, and their mass-loss rate will increase (e.g. Vassiliadis & Wood 1993). As a result, their optical magnitudes will become fainter due to their thicker dust shells, excluding them from the MACHO and OGLE databases. Infrared light curves are necessary to determine the periods for the reddest stars.

Table 2 also presents the periods of pulsation and the bolometric luminosity. We estimated the bolometric luminosity by summing the IRS spectrum from 5.1 to 36 μm and also summing linear interpolations through the photometry from Siding Spring Observatory. The photometric points generally lie at wavelengths affected by molecular absorption bands and thus lie well below the continuum, requiring a correction which typically raises the luminosity by $\sim$40%. We estimated the strength of this correction from the SWS sample of carbon stars (defined in §3.2) by summing the flux from 2.4 to 5.1 μm, which the IRS does not cover, and comparing it to the sum from 5.1 to 35 μm. The resulting correction is a smooth function of [6.4]−[9.3] color (defined in §3.1), and we estimated its strength for our SMC targets based on their color. We also extrapolate a Wien distribution to shorter wavelengths and a Rayleigh-Jeans tail to the red, but this modification has only a small effect on the luminosity. We have begun to fit our spectra using radiative transfer models, and while that work is still in its early stages, we can confirm that it produces luminosities typically within 10% of luminosities estimated here (the worst discrepancies are 25%). For all sources, the assumed distance modulus to the SMC is 18.9.

3. ANALYSIS

3.1. *The Manchester method*

Our analysis is based on the "Manchester method," which is designed to place the analyses of the samples of carbon stars presented here and by Zijlstra et al. (2006) on a common basis. The method defines two color indices, [6.4]−[9.3] and [16.5]−[21.5], to characterize the color temperature of the star-plus-dust system on the blue and red sides of the 11.3 μm SiC feature. Amorphous carbon dominates the dust emission, and its optical efficiency falls roughly as $\lambda^{-1.9}$, making it difficult to distinguish its emission from the stellar photosphere. That task requires radiative transfer modelling, which we leave for the future. In the following description, "continuum" refers to the combined spectrum of the star and the amorphous carbon. This method uses a simple scheme of fitting line segments under the narrow spectral features to approximate the "continuum."

The [6.4]−[9.3] color is calculated by separately summing the total spectral emission from 6.25 to 6.55 and 9.10 to 9.50 μm (see Figure 4). It serves as an indicator of the temperature of the carbon-rich dust and its contribution relative to the stellar contribution. In the analysis which follows, we use it to discriminate between optically thin, warm shells and optically thick, cool shells. The 6.4 μm band measures the continuum between the CO band at ∼5.0 μm and the C_2H_2 band at 7.5 μm, while the 9.3 μm band falls between the latter band and an absorption band at ∼10.0 μm which most likely arises from C_3 (Jørgensen et al. 2000).

The [16.5]−[21.5] color, measured over the wavelength ranges 16.0–17.0 and 21.0–22.0 μm, is the basis for estimating the cool dust temperature underlying the MgS feature, which extends from ∼24 μm past the red end of the LL spectral range (see Figure 5). While the IRS data provide a substantial improvement in sensitivity over the spectra from the SWS on *ISO*, the wavelength range is more limited. Data from LL are only usable out to ∼36 μm, while the SWS provided good coverage out to 45 μm. We have less information about the red side of the MgS feature, but we have improved the blue side, where data in Band 3E on the SWS (27–28 μm) proved to be of dubious quality.

Since we cannot observe the continuum to the red of the MgS feature, we extrapolate the continuum from the blue side assuming a Planck function with the temperature corresponding to the [16.5]−[21.5] color. The bandpasses for the 16.5 and 21.5 μm measurements were chosen to sample the continuum between the 13.7 μm C_2H_2 band and the blue end of the MgS feature at 24 μm, and they avoid any potential problems at the joint between LL orders 1 and 2 at ∼19–21 μm.

We measure the strength of the MgS feature by summing the flux from 24 to 36 μm above the extrapolated continuum. Any extrapolation method has its dangers, and our measurement of the MgS feature is more prone to error than our measurements of the C_2H_2 bands or the SiC feature. In some of the spectra, the observed spectrum in the 24–36 μm range actually passes *under* the extrapolated Planck function, emphasizing the limits of our method. In none of these cases does there appear to be a MgS dust feature in the spectrum. In other spectra (most notably MSX SMC 066), the spectrum continues to climb to the red edge of the LL wavelength range, suggesting that the long-wavelength excess is more likely a result of background contamination than MgS emission. Only six of the 19 sources in our SMC sample show a clear MgS feature with an upturn at 24 μm and a downturn at 36 μm. In the other cases, we have set the strength of the MgS feature to zero.

To measure the strengths of the C_2H_2 absorption bands at 7.5 and 13.7 μm and the SiC emission feature at 11.3 μm, we fit line segments to the continuum on either side and use this as an estimate of the continuum above or below the feature. For the molecular bands, we report equivalent widths (EW), while for the dust features, we report the ratio of their integrated flux to the integrated continuum flux. Table 3 provides the wavelengths used to estimate the continuum. The features were integrated between the continuum wavelengths.

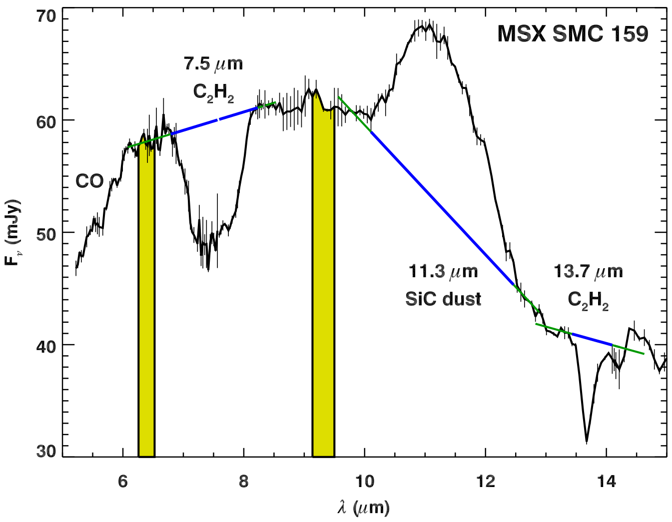

FIG. 4.— An example of the extraction of the molecular bands and the SiC dust feature from the spectrum of MSX SMC 159 using line segments to approximate a continuum. The vertical bars at 6.4 and 9.3 μm show the wavelength ranges used to determine the [6.4]−[9.3] color.

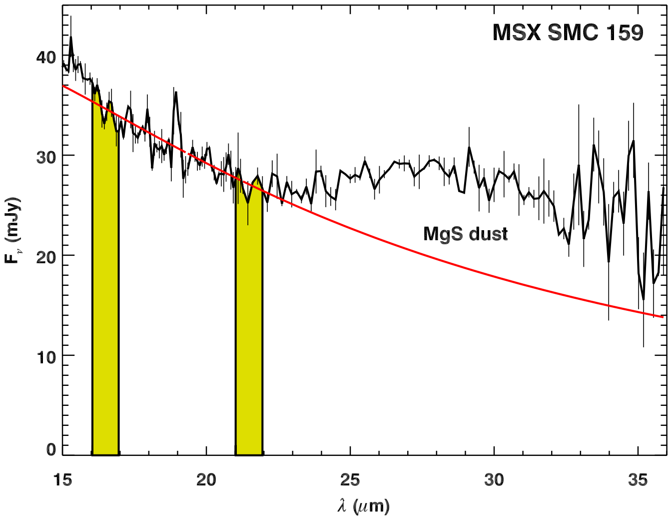

FIG. 5.— The extraction of the strength of the MgS dust feature, using MSX SMC 159 as an example. The vertical bars at 16.5 and 21.5 μm show the wavelength ranges used to measure the [16.5]−[21.5] color, from which we estimate a color temperature used to extrapolate the continuum underneath the MgS feature beyond 24 μm (dashed line).

TABLE 3
FITTING WAVELENGTHS

Feature	λ (μm)	Blue continuum (μm)	Red continuum (μm)
C_2H_2 abs.	7.5	6.08–6.77	8.25–8.55
SiC dust em.	11.3	9.50–10.10	12.50–12.90
C_2H_2 abs.	13.7	12.80–13.40	14.10–14.70

Figures 4 and 5 illustrate how we determine the colors and feature strengths using MSX SMC 159 as an example. For the SiC feature, we also determine the central wavelength, which is defined as that wavelength with equal amounts of flux from the feature to either side after continuum subtraction.

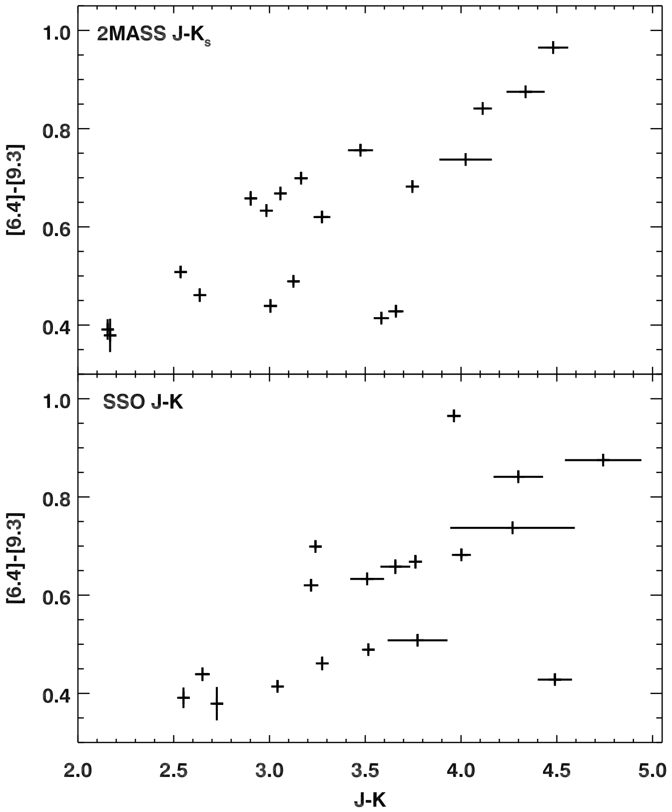

FIG. 6.— The [6.4]−[9.3] colors extracted from the spectra, plotted as a function of J−K color. The top panel plots the 2MASS J−K$_s$ color, and the bottom panel plots the SSO J−K color. In both cases, the [6.4]−[9.3] color correlates reasonably well with the near-infrared color. The overall shift between the two J−K colors results from the shift in the position of the J and K bands between the two systems. The two most notable outliers at J−K$_s$∼3.6 and [6.4]−[9.3]∼0.4 are MSX SMC 066 and 200. MSX SMC 200 is the only outlier when looking at SSO J−K color.

Figure 6 compares the [6.4]−[9.3] color measured from the spectra with the J−K color using both the 2MASS and SSO photometry. The apparent overall shift in J−K between the 2MASS and SSO systems is real; it arises from a shifts in the band centers. In the 2MASS system, the centers of the J and K$_s$ bands are 1.25 and 2.15 μm, respectively. In the SSO system, the J and K bands are shifted to 1.24 and 2.22 μm. The carbon stars in this sample are very red and far from Rayleigh-Jeans distributions, which accentuates the effect of moving the band centers.

The [6.4]−[9.3] color shows a correlation with J−K in both systems. The J−K color is more sensitive to photospheric emission, while the [6.4]−[9.3] colors is more sensitive to emission from the dust, so the scatter in the data is not surprising, even though the SSO photometry was obtained at the same phase as the spectra used to determine the [6.4]−[9.3] color. The two most significant outliers are MSX SMC 066 and 200. Both lie at J−K$_s$∼3.6 and [6.4]−[9.3]∼0.4. In the comparison with the SSO J−K color, only MSX SMC 200 remains an outlier.

Table 4 presents our measurements of the sample of 19 carbon stars in the SMC. We do not report a MgS strength unless we believe it be valid, and we do not report a central wavelength for SiC features too weak to be measured. Figures 7 and 8 plot the strengths of the molecular absorption bands and dust emission features, respectively, as a function of the [6.4]−[9.3] color.

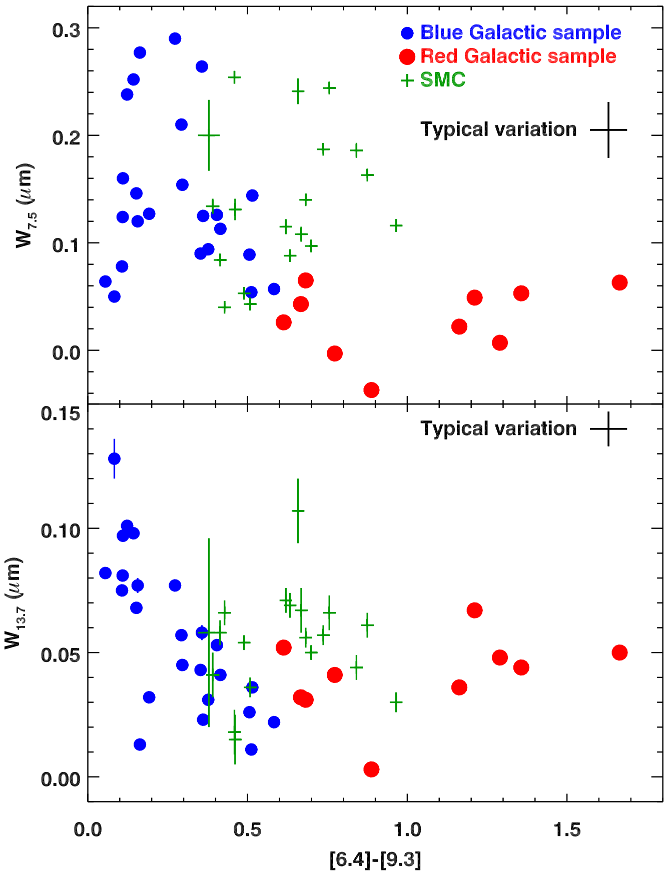

FIG. 7.— The equivalent widths of the C_2H_2 bands at 7.5 and 13.7 μm as a function of [6.4]−[9.3] color for both the SMC sample (plus signs) and the SWS Galactic sample (circles). The redder sources in the SMC sample show stronger absorption bands than their counterparts in the Galaxy. The black cross labelled "typical variation" reflects the expected impact on the data from the variability of the star, based on an analysis of those sources observed multiple times by the SWS.

3.2. *Control sample*

We have also analyzed the sample of carbon stars in the Galaxy observed by the SWS using the same method as described above. This sample includes a total of 63 spectra of 39 sources, consisting of 29 sources classified by Kraemer et al. (2002) as 2.CE (warm carbon-rich dust emission), four classified as 3.CE (cool carbon-rich dust emission), and six classified as 3.CR (cool and reddened carbon-rich dust emission). Two sources (S Cep and V460 Cyg) were observed twice, and four sources were observed several times each (V CrB, 6 times; V Cyg, 6; T Dra, 8; R Scl, 6). Five of the 2.CE spectra were dropped from the sample because they are too noisy for meaningful analysis.

In this paper, we concentrate on the properties of the SWS sample as a control group for our SMC sample. We will present a more detailed analysis of the Galactic sample elsewhere (Sloan et al. in preparation). Yang et al. (2004) have examined most of the spectra in this sample, and they have de-

TABLE 4
SPECTROSCOPIC RESULTS

MSX SMC	[6.4]−[9.3] (mag)	[16.5]−[21.5] (mag)	EW at 7.5 μm (μm)	EW at 13.7 μm (μm)	λ_{SiC} (μm)	SiC/continuum	MgS/continuum	Infrared Spec. Class
033	0.49±0.01	-0.06±0.03	0.053±0.004	0.054±0.003	11.34±0.06	0.036±0.003	···	2.CE
036	0.76±0.01	0.17±0.02	0.244±0.005	0.066±0.007	11.26±0.03	0.088±0.004	0.211±0.047	3.CE
044	0.51±0.01	-0.09±0.03	0.043±0.006	0.036±0.004	11.25±0.09	0.022±0.005	···	2.CE
054	0.74±0.01	0.16±0.02	0.187±0.004	0.057±0.004	11.27±0.02	0.179±0.004	0.116±0.027	3.CE
060	0.96±0.00	0.31±0.02	0.116±0.004	0.030±0.004	11.42±0.04	0.051±0.003	0.253±0.032	3.CR
062	0.67±0.01	0.24±0.02	0.108±0.007	0.067±0.009	11.23±0.07	0.066±0.005	···	3.CE
066	0.41±0.01	0.17±0.03	0.084±0.002	0.058±0.005	11.34±0.04	0.034±0.002	···	2.CE
091	0.66±0.01	0.15±0.04	0.241±0.012	0.107±0.013	11.30±0.05	0.148±0.010	···	3.CE
093	0.44±0.01	0.23±0.05	0.257±0.006	0.032±0.006	11.06±0.16	0.025±0.006	···	2.CE
105	0.84±0.01	0.25±0.02	0.186±0.007	0.044±0.005	11.22±0.02	0.154±0.006	0.253±0.028	3.CR
142	0.38±0.03	-0.23±0.22	0.200±0.033	0.058±0.038	···	0.018±0.018	···	2.CE
159	0.87±0.01	0.31±0.02	0.163±0.003	0.061±0.005	11.21±0.02	0.178±0.004	0.427±0.027	3.CR
162	0.46±0.01	0.06±0.12	0.131±0.010	0.015±0.010	11.31±0.09	0.059±0.007	···	2.CE
163	0.68±0.01	0.17±0.01	0.140±0.005	0.056±0.004	11.27±0.02	0.163±0.004	0.148±0.019	3.CE
198	0.62±0.01	0.09±0.02	0.115±0.007	0.071±0.005	11.19±0.05	0.049±0.003	···	3.CE
200	0.43±0.01	-0.11±0.03	0.040±0.004	0.066±0.005	11.44±0.18	0.009±0.003	···	2.CE
202	0.39±0.02	0.06±0.04	0.134±0.007	0.041±0.009	···	0.005±0.008	···	2.CE
209	0.70±0.01	0.12±0.03	0.097±0.005	0.050±0.003	11.16±0.05	0.028±0.002	···	3.CE
232	0.63±0.01	0.07±0.03	0.088±0.005	0.069±0.005	10.98±0.09	0.028±0.003	···	3.CE

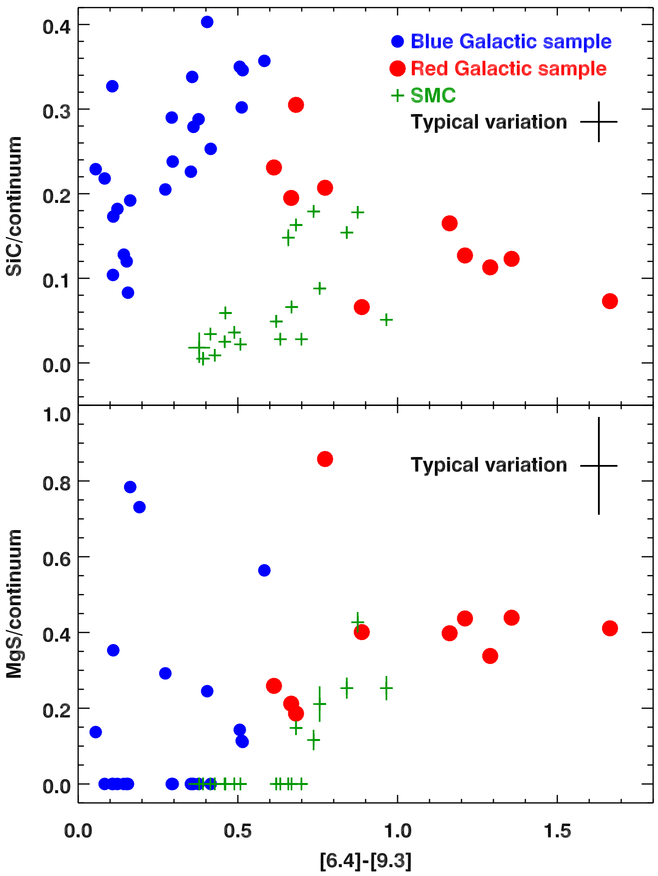

FIG. 8.— The strength of the dust emission features from SiC at 11.3 μm and MgS at ~30 μm as a function of [6.4]−[9.3] color. Symbols are as in Fig. 7. The SMC sample tends to show weaker dust emission than the Galactic sample.

veloped a classification system similar to ours, running from A to D for increasingly red sources. Hereafter, we will refer to the 24 2.CE sources as the blue Galactic sample, and the 10 3.CE and 3.CR sources as the red Galactic sample.

The boundary between the 2.CE and 3.CE sources in the Galactic sample lies at [6.4]−[9.3]=0.60, and similarly, a color of 0.80 separates the 3.CE and 3.CR sources. While the earlier classification of the SWS data (Kraemer et al. 2002) did not make use of the [6.4]−[9.3] color, we apply it here to distinguish these classes in the SMC sample. Table 4 includes these classifications.

For the sources observed multiple times, we generated and analyzed a co-added spectrum. We also examined the individual spectra to investigate how much the spectral properties of a given source can vary over a pulsation cycle. For each source, we determined the standard deviation of the various measured properties and from these determined a median variation, which appears in the relevant figures (7–10) as a black cross labelled “typical variation.”

4. RESULTS

4.1. *Molecular band strengths*

Figure 7 plots the equivalent widths of the C_2H_2 bands as a function of [6.4]−[9.3] color for both the SMC sample and the Galactic sample. At first thought, it might seem possible that the lower metallicities in the SMC would lead to optically thinner dust shells, which would make it easier to see through the dust envelope into the molecular absorption zone. We have accounted for this effect by plotting the band strengths as a function of [6.4]−[9.3] color, which serves as a proxy for the optical depth of the shell. For both the 7.5 and 13.7 μm bands, the two groups overlap significantly for [6.4]−[9.3] $<$ 0.6, but for thicker dust shells, the bands are stronger in the SMC sources.

In even the reddest sources in our Galactic sample, where the line of sight to the stellar photosphere should be veiled by the overlying dust, the molecular bands are present. It is unlikely that we are seeing down to the stellar photosphere in these cases; it is more likely that the absorbing molecules are in an extended envelope well above the stellar photosphere and overlapping with the circumstellar dust shell. Van Loon et al. (2006) use a similar argument to explain the strength and shape of the 3.1 and 3.8 μm bands due to C_2H_2 in a sample of carbon stars in the LMC.

The difference in band strength between the SMC and Galactic samples is more readily apparent at 7.5 μm than at 13.7 μm, probably because we are only measuring the narrow Q branch of the 13.7 μm feature. For high column densities, the Q branch will be saturated, and one would need to measure the broad P and R branches to determine the column density, but these branches are difficult to separate from the continuum. It should also be kept in mind that the 7.5 and 13.7 μm bands have different excitation energies, meaning that they sample different regions of the extended molecular envelope.

4.2. *The SiC dust emission feature*

The SiC dust emission feature at 11.3 μm lies between two molecular absorption bands, complicating our ability to accurately extract its strength. To the blue, we have the 10.0 μm absorption band attributed to C_3 (Jørgensen et al. 2000). This feature does not appear to be strong enough to have a significant impact on our spectra. The red side of the SiC feature is more of a problem, since the dust emission overlaps the P branch of the ν_5 band, which in some cases could extend past $\sim$12.5 μm (Aoki et al. 1999). If we fit the continuum too far to the red, then we are really fitting molecular absorption. Fitting too far to the blue cuts off dust emission. We have chosen the 12.5–12.9 μm range as a compromise. In our analysis, we have experimented with other wavelength ranges, and we have found that the conclusions we present below are robust in a qualitative sense. Some of the quantitative results, of course, do depend on where we fit the continuum.

The top panel of Figure 8 compares the strength of the SiC dust emission features in the Galactic sample and in the SMC. Five sources in the SMC, all with [6.4]$-$[9.3] $>$ 0.6, show SiC features stronger than 10% of the integrated continuum, similar in strength to their Galactic counterparts with the same colors. The remaining sources in the SMC sample, especially the blue sources, show comparatively weaker SiC features.

The apparent trend of decreasing SiC emission strength as a function of [6.4]$-$[9.3] color in the red Galactic sample must be considered with caution. While amorphous carbon dominates the dust in these shells, enough SiC dust can be present to force the 11.3 μm feature into absorption, as first suggested by Jones et al. (1978) and supported by the comparison of laboratory data with both ground-based observations (Speck et al. 1997) and *ISO*/SWS data (Clément et al. 2003). Thus, the apparent weakening of the SiC feature in the Galactic sample as the spectra get redder could in fact result from self-absorption in the feature.

The SiC feature is notorious for appearing at a wide range of wavelengths. While the emission feature typically appears at 11.3 μm, it can be seen out to 11.7 μm. In extreme carbon stars, the feature can appear in absorption, usually at $\sim$10.8 μm. Speck et al. (2005) have presented recent laboratory measurements to explain these wavelength shifts. SiC grains emit with two components, a longitudinal optic (LO) at 10.8 μm and a transverse optic (TO) to the red. As the SiC grains increase in size, the LO increases with respect to the TO, shifting the emission feature to the blue. Speck et al. (2005) explain the absorption at 10.8 μm as the result of different grain size distributions, with the cool absorbing component containing larger grains with an enhanced LO and the warmer emitting component containing smaller grains with an enhanced TO, shifting the feature from 11.3 μm to the red. If this scenario is valid, we can use wavelength to track the optical depth of the SiC feature.

Figure 9 illustrates how the apparent central wavelength of the SiC feature varies as a function of [6.4]$-$[9.3] color for the Galactic SWS sample. For colors from 0.0 to 0.5, the apparent central wavelength shows a great deal of scatter between values of 11.1 and 11.5 μm, but a general trend of decreasing wavelength with reddening color is noticeable. The Pearson correlation coefficient (e.g. Press et al. 1988) of a line segment fit to the blue of [6.4]$-$[9.3]=0.45 is 0.63, indicating a reasonable correlation despite the scatter. Beyond [6.4]$-$[9.3]=0.5, the apparent central wavelength increases monotonically to nearly 11.6 μm for the reddest source in our SWS sample. The correlation coefficient in this range is an impressive 0.95.

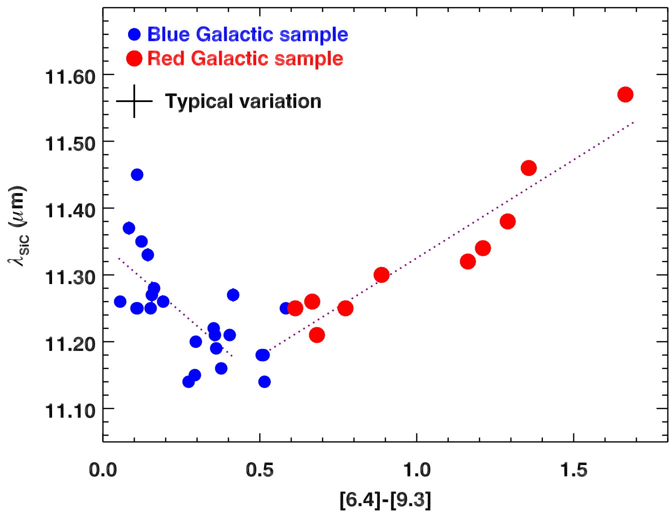

FIG. 9.— The apparent central wavelength of the SiC feature as a function of [6.4]$-$[9.3] color for the Galactic sample. Symbols are as defined in Fig. 7. The wavelength decreases from colors of 0.0 to 0.5, then increases steadily to almost 11.6 μm for the reddest source in our sample. The increase in apparent central wavelength for the red sources is consistent with the stronger self-absorption at 10.8 μm described by Speck et al. (2005). Line segments fitted to the data on either side of [6.4]$-$[9.3]=0.45 are shown as dotted lines.

In Figure 8 (top), the measured strength of the SiC emission generally increases with [6.4]$-$[9.3] for the blue Galactic sources (although there are a few notable outliers). The apparent turnover at [6.4]$-$[9.3]$\sim$0.5 and the subsequent drop in apparent strength in the Galactic sample can now be interpreted not as an intrinsic decline in SiC dust abundance, but as the growing effect of self-absorption on the measured strength.

Figure 10 compares the apparent central wavelength of the SiC feature (λ_{SiC}) in the Galactic and SMC samples. Two sources, MSX SMC 060 and 200, show central wavelengths $>$ 11.4 μm, but in MSX SMC 200, the uncertainty is nearly 0.2 μm. MSX SMC 060 has a central wavelength of 11.42 μm and a [6.4]$-$[9.3] color of 0.97. The strength of the SiC feature in its spectrum is lower than some of the bluer sources, making it probable that this source shows some mild effects from self-absorption. The remaining sources in the sample show no evidence for self absorption, leading us to conclude that as a group, the SMC spectra do indeed show less emission from SiC dust than their Galactic counterparts.

Even where the two samples show similar apparent strengths of the SiC feature, the Galactic sources have features shifted more to the red on average, indicating that they are more self-absorbed. Correcting for the effect of self-absorption on our measurements would make the two samples even more distinct.

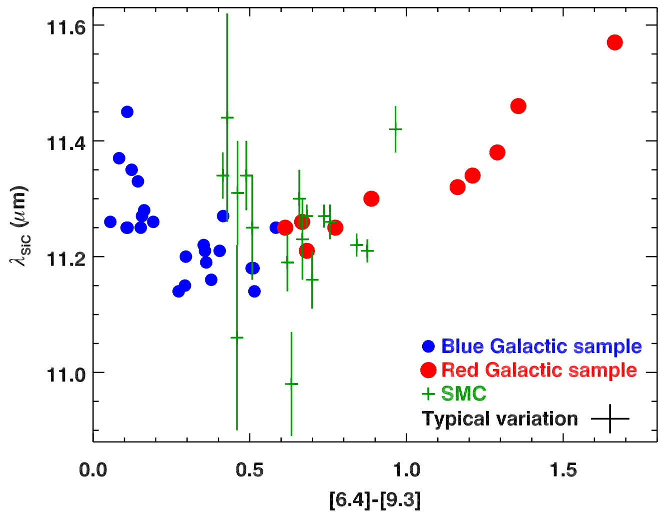

FIG. 10.— A comparison of the apparent central wavelength of the SiC feature for the Galactic and SMC samples, as in Fig. 9. Symbols are as in Fig. 7. The SMC sample occupies a tight wavelength range between 11.15 and 11.45 μm, with the exception of MSX SMC 093 and 232, which both show SiC features shifted to the blue. Few of the SMC sources show evidence of self-absorption in the SiC feature, which is consistent with the intrinsic weakness of this feature in the SMC sample compared to the Galactic sample.

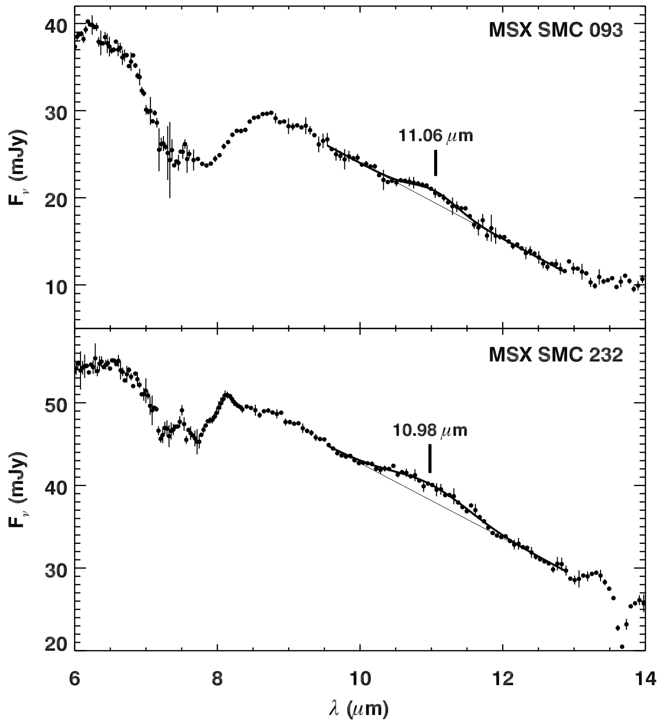

FIG. 11.— The spectra of MSX SMC 093 and 232, showing the weak and blue-shifted SiC features and the Gaussians fit to them. The data are plotted as filled circles with error bars, the fitted linear continua under the 11.0 μm emission features appear as thin lines, and the Gaussian fits as thick lines. The line centers, as marked, are at 11.06 and 10.98 for MSX SMC 093 and 232, respectively, while the Gaussians are centered at 11.05 and 11.00 μm, respectively.

Two of the sources, MSX SMC 093 and 232, are outliers in Figure 10, showing blue-shifted emission features peaking at 11.06 and 10.98 μm, respectively. Figure 11 shows these spectra, along with Gaussians fit to the features. The Gaussians are centered at 11.05 μm for MSX SMC 093 and 11.00 μm for MSX SMC 232. Because these features are weak compared to the continuum, their apparent position is somewhat sensitive to how we choose to fit the continuum. As an experiment, we changed the wavelength range for continuum fitting on the red side of the SiC feature to 12.0–12.9 μm. While the positions in the spectra of MSX SMC 093 and 232 remained within 0.02 μm, the SiC feature in MSX SMC 209 moved to 11.09$\pm$0.05 μm (from 11.16 μm), which would make it a third outlier in the sample.

Both MSX SMC 093 and 232 are among the four sources with the weakest measured SiC features. (MSX SMC 209 is as well.) Following the lead of Speck et al. (2005), we hypothesize that the emission from these grains is dominated by the longitudinal optic (LO), which indicates that the grains are larger than usually seen. Thus, these spectra show the enigmatic combination of both fewer and larger SiC grains.

A similar process might explain the overall trend apparent in the blue Galactic sources of decreasing central wavelength until the [6.4]$-$[9.3] color reaches $\sim$0.5. In this case, the trend of increasing grain size with increasingly red colors and thus growing optical depth makes more sense.

4.3. *The MgS dust emission feature*

Only one third of our sample shows an unambiguous MgS feature. Some spectra (such as MSX SMC 066, 142, and 209), appear to be contaminated by background emission which would hide any MgS feature, but the majority of the remaining 12 spectra simply show no evidence of MgS emission above the continuum extrapolated from the 16–22 μm region.

None of the SMC spectra with [6.4]$-$[9.3]<0.75 show a MgS feature, while at least some Galactic spectra show a feature throughout the range of colors. For the six spectra which do show MgS features, five have weaker features than their Galactic counterparts with similar colors. While the SMC spectra are generally noisy in this spectral range and sometimes contaminated by background emission, and our extrapolation method does have its limits, it still seems that the MgS feature is weaker in the SMC sample than in the Galactic sample.

5. DISCUSSION

5.1. *Dust emission and abundances*

Both the SiC and MgS dust emission features tend to be weaker in the carbon stars in the SMC than in the Galaxy. The most straightforward explanation for these differences is that they result from the lower metallicity in the SMC. Mg, Si, and S are all products of α-capture, and studies of halo stars show that the abundances of these elements behave similarly, decreasing as iron abundance decreases (See the review by Wheeler et al. 1989).

The sample of carbon stars in the SMC divides easily into three groups. Eight sources, which we call the blue sources, have 0.3<[6.4]$-$[9.3]<0.6, and all show weak SiC emission. The red sources (0.6<[6.4]$-$[9.3]<1.0), separate into two groups, six sources with weak SiC features, and five with strong SiC features. Table 5 compares the mean strength of the SiC features and mean color in these groups to groups from the Galactic sample with the same color ranges. The Galactic sample does not show a dichotomy in SiC strength among the red sources like the SMC sample.

The strength of the SiC feature in the SMC sample, compared to the Galactic sample, is down by a factor of 12 for the blue sources, 4 for the red sources with weak SiC features, and

TABLE 5
MEAN SiC STRENGTHS

Sample	N	<[6.4]−[9.3]>	<SiC/continuum>
Galactic blue	10	0.44	0.314±0.054
SMC blue	8	0.44	0.026±0.017
Galactic red	5	0.73	0.201±0.087
SMC red, weak SiC	6	0.72	0.052±0.023
SMC red, strong SiC	5	0.76	0.164±0.014

1.2 for the red sources with a strong SiC feature. Our measurements of the SiC feature in the red sources in the Galactic sample may be underestimated due to self-absorption, so the difference between the two samples may actually be larger. Abundances of Mg and Si in the SMC are about 15% of their Solar values, based on measurements of the H II region N88a (Kurt et al. 1999) and B supergiants (Lennon et al. 2003; Trundle et al. 2004; Dufton et al. 2005). Our measured dust strengths are roughly consistent with these abundance differences. The lower SiC strengths in the bluer sources could be explained if they representd an older and more metal-poor sample.

5.2. *The strong SiC sources*

The five sources in the SMC sample which show SiC emission nearly as strong as their Galactic counterparts are MSX SMC 054, 091, 105, 159, and 163. Four of these sources are also among the six showing a measurable MgS feature; MSX SMC 091 is the exception. Conversely, MSX SMC 036 and 060 are the two MgS sources which don't show strong SiC bands. As Figure 8 shows, the five strong SiC sources are all in the redder half of the sample in [6.4]−[9.3] color. The MgS sources are grouped even more clearly; the six reddest sources all show MgS features.

Figure 12 (top) shows that the strong SiC sources also tend to have the reddest J−K colors. Four of these sources are among the five reddest. MSX SMC 091, again, is the exception, although it is still redder than half the sample. The one red source with J−K > 4 but without strong SiC emission is MSX SMC 200. Figure 12 uses the photometry from SSO. The 2MASS photometry from an earlier epoch gives similar results, except that MSX SMC 060 is the one weak SiC source among the reddest five in J−K. We have noted above that MSX SMC 060 and 200 have the most red-shifted SiC features in our sample; we could possibly be underestimating the strength of these features due to self-absorption. The middle panel of Figure 12 shows that the strong SiC sources are also among the redder sources in K−L, although the trend is not as obvious as it is in J−K.

Given that the weakness of the SiC and MgS features in the general sample is consistent with the expected lower abundances of α-capture products in the SMC, it is conceivable that the sources with stronger SiC features differ from the rest of the SMC sample by having enhanced metallicities. If the metallicities resulted from comparative youth, then they might be located near younger clusters in the SMC, but there is nothing significant about their locations in the SMC. Younger stars would have a higher mass, and on average, they might show a higher luminosity. However, as the bottom panel of Figure 12 shows, only one of the eight sources with a bolometric luminosity > 10^4 $L_\odot$ has a strong SiC feature.

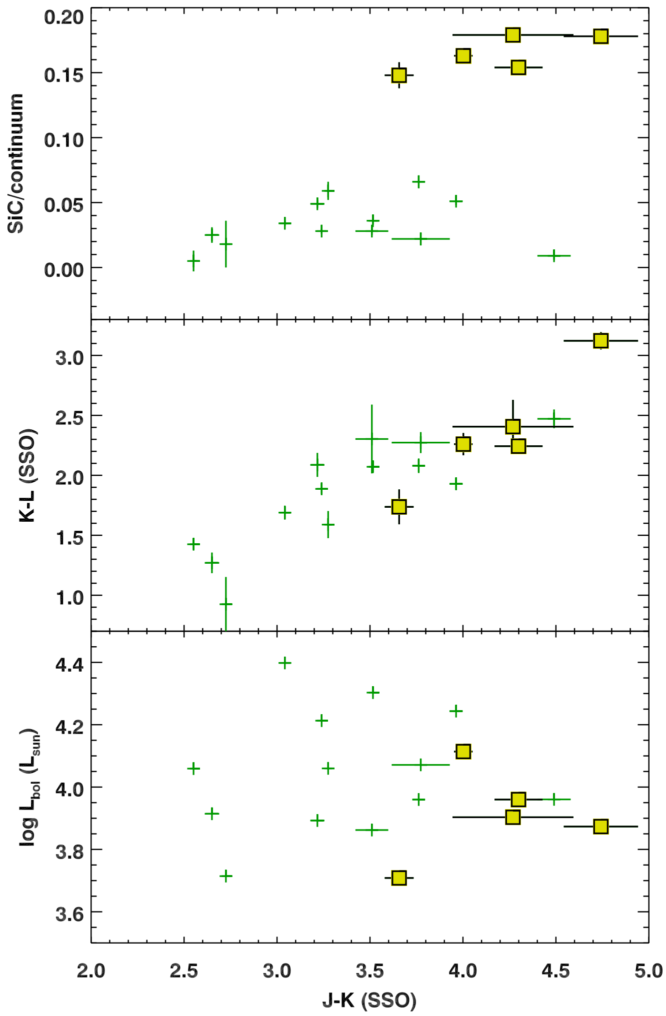

FIG. 12.— The strength of the SiC dust emission as a function of J−K color (*top*), our sample plotted on a JKL color-color diagram (*middle*), and bolometric luminosity vs. J−K color (*bottom*). The strong SiC sources are plotted with boxes. The photometry is from Siding Spring Observatory (SSO), although it should be noted that the dependence on 2MASS J−K_s colors is similar. The strong SiC sources tend to be among the redder sources in our sample, especially at J−K. §2.4 explains how we estimated the bolometric luminosity. The strong SiC sources are not among the brightest sources in the sample.

The strong SiC sources cover a wide range of luminosities, although four of the five tend to cluster in the lower half of the luminosity range.

The only clear distinctions between the strong SiC sources and the remaining carbon stars are that they (1) tend to also show MgS dust and (2) tend to be redder than the remaining sample at J−K and to a lesser degree, K−L and [6.4]−[9.3]. These redder colors imply a greater amount of amorphous carbon in their dust shells.

5.3. *Other unusual sources*

The star MSX SMC 060 shows a rather unusual lightcurve (Figure 3), and it has the reddest [6.4]−[9.3] color in our sample of carbon stars. It shows evidence for a long period of about 450–600 days, and when it is bright it shows a typical semi-regular (low overtone) pulsation with a period of 70–85 days. In some ways, this star is like an R CrB star, undergoing episodic dimming events, a slow recovery, and then showing semi-regular pulsation when it is optically bright. Photometrically, it is certainly as red in J−K and [6.4]−[9.3] as the two R CrB stars in the SMC observed with the IRS (Kraemer et al. 2005), MSX SMC 014 and 155. They have [6.4]−[9.3] = 0.92 and 0.77, respectively, compared to 0.96 for MSX SMC 060. The similarities in the light curve and photometry are interesting, even though the infrared spectrum of MSX SMC 060 differs significantly from the R CrB stars, which show relatively featureless spectra, while MSX SMC 060 has clear acetylene bands, strong MgS dust emission, and moderate (or possibly self-absorbed) SiC dust emission.

Two sources in Figure 6 do not follow the general relation between [6.4]−[9.3] and J−K_s colors, showing bluer colors at [6.4]−[9.3] than expected from the J−K colors in the 2MASS epoch. They are MSX SMC 066 and 200, and they have J−K_s colors in the 2MASS epoch of 3.58 and 3.66, respectively. In the SSO photometry, MSX SMC 066 has dropped to J−K = 3.04, among the bluest colors in our sample, while MSX SMC 200 has reddened to 4.49, among the reddest colors in our sample. The variability of MSX SMC 066 might explain why it stands out in Figure 6, but MSX SMC 200 has remained red at J−K, making its blue [6.4]−[9.3] color more difficult to explain.

The two sources illustrated in Figure 11, MSX SMC 093 and 232, are outliers in Figure 10 because their SiC features have shifted from ∼11.3 μm to ∼11.0 μm. As explained in §4.2, this shift may arise from an increased size in the emitting grains, even though the SiC dust is more optically thin.

5.4. *Acetylene and amorphous carbon*

5.4.1. *C/O ratio*

The C_2H_2 absorption bands are stronger in the SMC sample than in the Galactic sample, indicating that these molecules are more abundant in the atmospheres and outflows of carbon stars in the SMC. This result reinforces previous results based on 3–4-μm spectra of carbon stars in the Magellanic Clouds and the Sagittarius Dwarf Spheroidal galaxy (van Loon et al. 1999; Matsuura et al. 2002, 2005). These papers suggest that the increased abundance of C_2H_2 results from a higher C/O ratio in low-metallicity carbon stars, which arises for two reasons. First, as the metallicity drops, the dredge-ups will grow more efficient (Wood 1981), injecting more carbon into the atmosphere. Second, low-metallicity AGB stars have a lower oxygen abundance to begin with, increasing the C/O ratio for a given amount of dredged up carbon (Lattanzio & Wood 2004).

The analysis in this paper uses the [6.4]−[9.3] color as a proxy for the relative contributions of emission from the amorphous carbon dust and the stellar photosphere. Figure 7 shows that at a given [6.4]−[9.3] color, carbon stars in the SMC have more acetylene absorption than their Galactic counterparts. Thus, if our assumptions are correct, the carbon stars in the SMC have more acetylene around them than carbon stars *with the same amount of dust* in the Galaxy.

5.4.2. *Dust formation efficiency*

Allamandola et al. (1989) suggested acetylene as a probable building block of aromatic hydrocarbons in circumstellar shells, and numerical models support this mechanism (Frenklach & Feigelson 1989; Cherchneff 1992). Carbonaceous grains with a mixture of aliphatic and aromatic bonds can also be produced from acetylene, as shown by Kovačavić et al. (2003, 2005). The acetylene probably does not condense directly into solid material. A nucleation site provides a surface for the formation of carbonaceous solids in the outflows from carbon stars, and Frenklach et al. (1989) and Cadwell et al. (1994) have identified SiC as the most likely nucleation site.

TABLE 6
MEAN ACETYLENE STRENGTHS IN THE SMC

Sample	N	<EW at 7.5 μm> (μm)	<EW at 13.7 μm> (μm)
weak SiC	6	0.141±0.069	0.053±0.017
strong SiC	5	0.183±0.038	0.064±0.024

Our observations of the SMC reveal less SiC and MgS in the dust compared to the Galactic sample, raising another possible explanation for the excess acetylene seen in the SMC spectra besides the higher expected C/O ratios. The lower metallicity in the SMC leads to lower abundances of heavier elements such as Si, Mg, and S and fewer related dust grains. With less SiC to form the nuclei for the condensation of carbon, the dust formation may be less efficient, which might in turn explain the deeper acetylene absorption for a given amount of carbon-rich dust in the SMC (Figure 7).

While this scenario seems plausible, the five strong SiC sources in our sample do not follow the expected trend. Since the SiC emission in these sources is nearly as strong as the Galactic sources, one might expect more efficient dust formation to leave less acetylene compared to the sources with weaker SiC features. Table 6 compares the mean band strengths for the acetylene in the strong SiC sources to the same control sample of weak SiC sources in Table 5. The distributions of the molecular band strengths overlap significantly. If anything, the strong SiC emitters have stronger absorption bands. While the five strong SiC sources do not seem to support the scenario we propose, one must keep in mind that we have been unable to determine why these sources have so much SiC in their dust shells. They may represent an unusual population and thus make a poor test sample. The trends when comparing the overall Galactic and SMC samples are still clear.

We have been careful to base our comparisons on sources with similar amounts of dust, which is quite different from a comparison of the amount of dust produced by similar sources in the SMC and the Galaxy. A definitive answer will require radiative transfer modelling to properly measure the amount of amorphous carbon dust and a careful assessment of the luminosities and pulsational properties of the stars. We leave that work to the future, but we note in the meantime that the IRS spectra and the derived [6.4]−[9.3] colors clearly indicate that carbon stars in the SMC are capable of producing significant quantities of dust.

6. CONCLUSIONS

Analyzing the strength of identifiable spectral features as a function of [6.4]−[9.3] color allows us to separate the sample on the basis of the optical depth through the dust shell, which is effectively a measure of the amount of amorphous carbon around the star. Thus we can compare the carbon stars in the SMC sample to sources with a similar amount of circumstellar dust in the Galactic sample.

Carbon stars in the SMC have lower abundances of SiC and MgS dust compared to the amorphous carbon dust than their

Galactic counterparts. This result demonstrates that the nature of the dust produced by stars on the AGB can vary measurably with their initial metallicity.

Our observations of molecular band strengths confirm the shorter-wavelength results of van Loon et al. (1999) and Matsuura et al. (2002, 2005) who showed that stars with lower metallicities actually produce deeper acetylene absorption bands. They attributed this unexpected result to significantly higher C/O ratios in these stars. We have made our comparison on the basis of the [6.4]−[9.3] color, allowing us to conclude that stars surrounded by similar amounts of dust have more acetylene around them in the SMC than in the Galaxy, and have proposed an alternative scenario. The lack of SiC dust in the shells may deprive the amorphous carbon of seeds, lead to less efficient dust formation, and result in a higher ratio of acetylene to amorphous carbon.

Finally, we note that the combination of our results and previous work suggest that more carbon-rich dust should be injected into the ISM in a more metal-poor galaxy. First, a higher fraction of the stars evolve into carbon stars. Second, individual carbon stars in these metal-poor systems produce quantities of dust comparable to their Galactic counterparts, as our spectroscopy has shown. Finally, oxygen-rich stars should not produce as much dust, since the limiting factors will be the abundances of heavier elements like Mg, Al, Si, and Fe, all of which will be reduced in low-metallicity environments. Since amorphous carbon is the likely building block for PAH molecules, this result has important implications for the study of the emission features produced by these molecules in distant and/or metal-poor galaxies.

We gratefully acknowledge the referee, J. van Loon, whose thorough commentary has helped us to substantially improve this paper, and A. A. Zijlstra, whose input also proved most valuable. Support for G. C. S. was provided by NASA through Contract Number 1257184 issued by the Jet Propulsion Laboratory, California Institute of Technology under NASA contract 1407. M. M. is supported by the PPARC. The Australian Research Council provided support to P. R. W. This research has made use of the SIMBAD and VIZIER databases, operated at the Centre de Données astronomiques de Strasbourg, and the Infrared Science Archive at the Infrared Processing and Analysis Center, which is operated by JPL.

REFERENCES

Alcock, C., et al. 1996, ApJ, 461, 84
Allamandola, L. J., Tielens, A. G. G. M., & Barker, J. R. 1989, ApJS, 71, 733
Aoki, W., Tsuji, T., & Ohnaka, K. 1998, A&A, 340, 222
Aoki, W., Tsuji, T., & Ohnaka, K. 1999, A&A, 350, 945
Blanco, B. M., Blanco, V. M., & McCarthy, M. F. 1978, Nature, 271, 638
Blanco, B. M., Blanco, V. M., & McCarthy, M. F. 1980, ApJ, 242, 938
Cadwell, B. J., Wang, H., Feigelson, E. D., & Frenklach, M. 1994, ApJ, 429, 285
Cherchneff, I., Barker, J. R., & Tielens, A. G. G. M. 1992, ApJ, 401, 269
Clément, D., Mutschke, H., Klein, R., & Henning, Th. 2003, ApJ, 594, 642
Dufton, P. L., Ryans, R. S. L., Trundle, C., Lennon, D. J., Hubeny, L., Lanz, T., & Allende Prieto, C. 2005, A&A, 434, 1125
Egan, M. P., & Price, S. D., 1996, AJ, 112, 2862
Egan, M. P., Van Dyk, S. D., & Price, S. D. 2001, AJ, 122, 1844
Egan, M. P., et al. 2003, "The Midcourse Space Experiment Point Source Catalog, Version 2.3, Explanatory Guide," Air Force Research Laboratory Technical Report AFRL-VS-TR-2003-1589
Forrest, W. J., Houck, J. R., & McCarthy, J. F. 1981, ApJ, 248, 195
Frenklach, M., Carmer, C. S., & Feigelson, E. D. 1989, Nature, 339, 196
Frenklach, M. & Feigelson, E. D. 1989, ApJ, 341, 372
Gehrz, R. D., 1989, in Interstellar Dust, Proc. IAU Symp. 135, ed. L. J. Allamandola & A. G. G. M. Tielens (Dordrecht: Kluwer), 445
Gilman, R. C. 1969, ApJ, 155, L185
Goebel, J. H. & Moseley, S. H. 1985, ApJ, 290, L35
Griffin, I. P. 1990, MNRAS, 247, 591
Hackwell, J. A. 1972, A&A, 21, 239
Hill, V., Barbuy, B., & Spite, M. 1997, A&A, 323, 461
Hony, S., Waters, L. B. F. M., & Tielens, A. G. G. M. 2002, A&A, 390, 533
Houck, J. R., et al. 2004, ApJS, 154, 18
IRAS Science Team 1986, A&AS, 65, 607 (LRS Atlas)
Jones, B., Merrill, K. M., Puetter, R. C., & Willner, S. P. 1978, AJ, 83, 1437
Jørgensen, U. G., Hron, J., & Loidl, R. 2000, A&A, 356, 253
Kovačavić, E., Stefanović, I., Berndt, J., & Winter, J. 2003, J. Appl. Phys., 93, 2924
Kovačavić, E., Stefanović, I., Berndt, J., Pendleton, Y. J., & Winter, J. 2005, ApJ, 623, 242
Kraemer, K. E., Sloan, G. C., Price, S. D., & Walker, H. J. 2002, ApJS, 140, 389
Kraemer, K. E., Sloan, G. C., Wood, P. R., Price, S. D., & Egan, M. P. 2005, ApJ, 631, L147
Kurt, C. M., Dufour, R. J., Garnett, D. R., Skillman, E. D., Mathis, J. R., Peimbert, M., Torres-Peimbert, S., & Ruiz, M.-T. 1999, ApJ, 518, 246
Lattanzio, J. C. & Wood, P. R. 2004, "Evolution, Nucleosynthesis and Pulsation of AGB Stars," in Asymptotic Giant Branch Stars, ed. H. J. Habing & H. Olofsson, A&A Library (New York: Springer), 23
Lennon, D. J., Dufton, P. L., & Crowley, C. 2003, A&A, 398, 455
Luck, R. E., Moffett, T. J., Barnes, T. G., III, & Gieren, W. P. 1998, AJ, 115, 605
McGregor, P. J. 1994, PASP, 106, 508
McGregor, P. J., Hart, J., Hoadley, D., & Bloxham, G. 1994, in Infrared Astronomy with Arrays, ed. I McLean (Dordrecht: Kluwer), 299
Martin P. G. & Rogers C. 1987, ApJ, 322, 374
Matsuura, M., Zijlstra, A. A., van Loon, J. Th., Yamamura, I., Markwick, A. J., Woods, P. M., & Waters, L. B. F. M. 2002, ApJ, 580, L133
Matsuura, M., Zijlstra, A. A., van Loon, J. Th., Yamamura, I., Markwick, A. J., Whitelock, P. A., Woods, P. M., Marshall, J.R., Feast, M. W. & Waters, L. B. F. M. 2005, A&A, 434, 706
Matsuura, M., et al. 2006, MNRAS, submitted
Olivier, E. A. & Wood, P. R. 2005, MNRAS, 362, 1396
Press, W. H., Flannery, B. P., Teukolsky, S. A., & Vetterling, W. T. 1988, Numerical Recipes in C (Cambridge: Cambridge Univ. Press)
Renzini, A. & Voli, M. 1981, A&A, 94, 175
Russell, S. G. & Bessell, M. S. 1989, ApJS, 70, 865
Skrutskie, M. F., et al. 2006, AJ, 131, 1163
Sloan, G. C., Spoon, H. W. W., & Bernard-Salas, J. 2005, IRS Technical Report 05002, Low-resolution wavelength calibration of the IRS (Ithaca, NY: Cornell, available at http://isc.astro.cornell.edu/tech/tr/)
Sloan G. C. & Egan M. P. 1995, ApJ, 444, 452
Smith, V. V., et al. 2002, AJ, 124, 3241
Speck, A. K., Barlow, M. J. & Skinner, C. J. 1997, MNRAS, 288, 431
Speck, A. K., Thompson, G. D., & Hofmeister, A. M. 2005, ApJ, 634, 426
Szymański, M. K. 2005, Acta Astron., 55, 43
Treffers, R. & Cohen, M. 1974, ApJ, 188, 545
Trundle, C., Lennon, D. J., Puls, J., Dufton, P. L. 2004, A&A, 417, 217
Udalski, A., Kubiak, M., & Szymánski, M. 1997, Acta Astron., 47, 319
van Loon, J. Th., Zijlstra, A. A., Whitelock, P. A., Waters, L. B. F. M., Loup, C., & Trams, N. R. 1997 A&A, 325, 585
van Loon, J. Th., Zijlstra, A. A., & Groenewegen, M. A. T. 1999, A&A, 346, 805
van Loon, J. Th., Marshall, J. R., Cohen, M., Matsuura, M., Wood, P. R., Yamamura, I., Zijlstra, A. A. 2006, A&A, 447, 971
Vassiliadis, E. & Wood P. R. 1993, ApJ, 413, 641
Werner, M. W., et al. 2004, ApJS, 154, 1
Wheeler, J. C., Sneden, C., & Truran, J. W., Jr. 1989, ARA&A, 27, 279
Whitelock, P. A., Feast, M. W., van Loon, J. Th., & Zijlstra, A. A. 2003, MNRAS, 342, 86
Wood, P. R. 1981, in Physical Processes in Red Giants, ed. I. Iben & A. Renzini, (Dordrecht: Reidel), 135
Wood, P. R. 2998, A&A, 338, 592
Wood, P. R. 2003, in Mass-Losing Pulsating Stars and their Circumstellar Matter, ed. Y. Nakada, M. Honma & M. Seki, (Dordrecht: Kluwer), 3
Wood, P. R., Whiteoak, J. B., Hughes, S. M. G., Bessell, M. S., Gardner, F. F., & Hyland, A. R. 1992, ApJ, 397, 552
Yang, X., Chen, P., & He, J. 2004, A&A, 414, 1049
Zijlstra, A. A., et al. 2006, MNRAS, submitted